EFFECT OF SOLIDIFICATION CONDITIONS ON THE MICROSTRUCTURE OF MULTIPHASE $Al_{0.4}CoCr_{1.3}FeNi_{1.3}(Si, Ti, C, B)_{0.4}$ COMPLEX CONCENTRATED ALLOY

Alena KLIMOVÁ, Juraj LAPIN

Institute of Materials and Machine Mechanics, Slovak Academy of Sciences, Slovak Republic, EU,
alena.klimova@savba.sk

https://doi.org/10.37904/metal.2023.4667

Abstract

Complex concentrated alloy (CCA) with a nominal composition $Al_{0.4}CoCr_{1.3}FeNi_{1.3}(Si, Ti, C, B)_{0.4}$ was prepared at two different solidification conditions. Centrifugal casting (CC) of the CCA was applied due to the turbulent filling of a graphite mould at non-steady solidification conditions and directional solidification (DS) was performed at steady-state solidification conditions. Directional solidification was carried out in a Bridgman-type apparatus at a constant growth rate of 1.39 x 10^{-5} $m \cdot s^{-1}$ and a constant temperature gradient in liquid. Both types of ingots were subjected to microstructural analysis using light microscopy (LM) and scanning electron microscopy (SEM). The chemical composition of the coexisting phases was measured by energy-dispersive spectrometry (EDS). Segregation of Al, Si, Ti, B and C to the interdendritic region during solidification leads to the formation of several interdendritic phases identified in the ingots. The effect of solidification conditions on the size of dendrites and interdendritic phases was evaluated. Isothermal annealing at 1260 °C leads to the melting of all interdendritic phases. Effective partition coefficients of alloying elements were calculated from the measured chemical composition of dendrites and interdendritic region in samples annealed at 1260 °C for 1 h followed by water quenching.

Keywords: Complex concentrated alloys, solidification, microstructure, segregation

1. INTRODUCTION

A new alloy-design concept of multi-principal alloys with a high configuration entropy termed high entropy alloys (HEAs) was introduced by Cantor [1] and Yeh [2] around 20 years ago. Besides the original HEAs with the strict requirements for more than 5 elements, almost equiatomic composition and simple single-phase structure another group of multi-component alloys derived from HEAs named compositionally complex alloys or complex concentrated alloys (CCAs) appeared [3]. The CCAs have been designed to improve the microstructure and mechanical properties of single-phase HEAs for a wider range of structural applications. These CCAs include also multi-phase systems with complex types of structures. Among the large number of CCAs, the $Al_xCoCrFeNi$ system (x = 0 - 1 molar ratio) as a member of 3d transition metal CCAs, belongs to the most widely studied [3]. According to the thermodynamic calculations and numerous experimental investigations, in dependence on Al content and applied heat treatments, the single-phase (FCC(A1) or BCC(B2)), duplex or multi-phase microstructures consisting of various combinations of FCC(A1), BCC(A2), BCC(B2), σ and $L1_2$ crystal structure were identified in this system [4-6]. Solidification of $Al_xCoCrFeNi$ alloys leads usually to the formation of a dendritic type of structure [7]. Partitioning of Al to the last interdendritic liquid in $Al_{0.5}CoCrFeNi$ alloy changes into its opposite segregation behaviour in equimolar AlCoCrFeNi [4]. In the duplex FCC(A1)+BCC(B2) structures, the FCC(A1) is enriched by Fe and Cr, while BCC(B2) is enriched by Al and Ni. In the multiphase $Al_xCoCrFeNi$ alloys Cr and Fe segregate into the disordered BCC(A2) phase, Al, Ni and Co into the ordered BCC(B2) [8]. Minor additions of other elements such as B [9], C [10], Ti [10-11] and Si [12] were introduced to the $Al_xCoCrFeNi$ system by several researchers to improve mechanical properties, wear, and corrosion resistance. However, the mutual effect of all four additions B, C, Ti and Si has been studied in detail only for gravity - cast $Al_{0.4}Co_{0.9}Cr_{1.2}Fe_{0.9}Ni_{1.2}(Si, Ti, C, B)_{0.375}$ complex concentrated alloy (CCA) by Lapin et al. [13].

Controlled growth conditions during directional solidification are usually used for the purpose to investigate the fundamental aspects of the microstructure formation and microsegregation evolution of alloying elements as well as to achieve a preferred crystallographic orientation and required microstructure for optimization of the mechanical properties. In the case of the $Al_xCoCrFeNi$ system, Bridgman solidification of the equimolar AlCoCrFeNi with BCC(A2)/BCC(B2) structure was investigated by several authors [14,15] to study the effect of growth rate (V) on the morphology of solid-liquid interface (transition from planar to dendritic) and the influence of the temperature gradient (G) to the growth rate ratio (G/V) on the morphology transition from columnar to equiaxed grains, respectively. Multiphase $Al_{0.7}CoCrFeNi$ CCA showed a unique lamellar-dendrite microstructure composed of FCC(A1) + BCC(A2) + BCC(B2) phases over a wide range of cooling rates after directional solidification [16]. The increasing growth rate resulted in the decreasing spacing of FCC(A1)/BCC(B2) lamellae within the dendrites. As was reported by Ma et al. [17], Bridgman solidification is a suitable method for the preparation of $Al_{0.3}CoCrFeNi$ CCA with a single-crystal FCC(A1) structure and outstanding tensile ductility.

In the present paper, multiphase $Al_{0.4}CoCr_{1.3}FeNi_{1.3}(Si, Ti, C, B)_{0.4}$ complex concentrated alloy was subjected to experimental investigation. The solidification behaviour of this alloy was studied during centrifugal casting characterised by the turbulent filling of the mould as well as during directional solidification carried out at steady-state solidification conditions in the Bridgman-type apparatus. The effect of solidification conditions on the microstructure formation and microsegregation behaviour of alloying elements is discussed.

2. EXPERIMENTAL PROCEDURE

The studied CCA with a nominal chemical composition $Al_{0.4}CoCr_{1.3}FeNi_{1.3}(Si, Ti, C, B)_{0.4}$ (molar ratio) was prepared by vacuum induction melting of master Ni alloy and high purity elements (Fe, Co, Cr, Al) in Al_2O_3 crucible followed by tilt casting into the graphite mould. The as-cast cylindrical ingot was cut into smaller pieces, which were adjusted for directional solidification and centrifugal casting experiments. Directional solidification at steady-state conditions was performed in a Bridgman-type apparatus at a constant growth rate of V = 1.39 x 10^{-5} m·s^{-1} and constant temperature gradient in liquid at the solid-liquid interface of G_L = 16.5 x 10^3 K·m^{-1}. The length of the directionally solidified (DS) ingot with the diameter of 15 mm was 152 mm. The vacuum induction melting of the charge for centrifugal casting (CC) was carried out in Al_2O_3 crucibles and the melt was poured into a graphite mould. The length and min/max diameter of a conical CC ingot was 178 mm and 14/17 mm, respectively. The samples cut from both types of ingots were used for the evaluation of the microstructure after solidification. The samples for determination of the microsegregation behaviour of alloying elements were annealed at 1260 °C for 1 h under an argon atmosphere and consequently quenched into the water. Standard metallographic techniques such as grinding on SiC papers, polishing on diamond paste with various grain sizes ranging from 10 to 0.25 μm and etching in a solution of 6 ml HNO_3, 3 ml HF and 100 ml H_2O were used. Microstructure investigations were performed by light microscopy (LM), scanning electron microscopy (SEM), and X-ray diffraction analysis (XRD). The XRD analysis was carried out by a diffractometer equipped with an X-ray tube and a rotating Cu anode operating at 12 kW. The chemical composition of the ingots was analysed by energy-dispersive spectrometry (EDS). The average content of carbon in the samples was measured by LECO CS844 elemental analyser. The average content of boron was calculated based on the certified composition of the master Ni alloy.

3. RESULTS AND DISCUSSION

3.1 Chemistry and microstructure of DS and CC samples

The nominal and measured chemical compositions of the CC and DS samples are summarised in **Table 1**. The measured values of the content of alloying elements correspond very well to the nominal ones and all observed differences fall only within standard deviations of the applied measurement methods.

Table 1 Nominal and measured chemical composition of DS and CC samples (at.%)

Sample	Co	Cr	Fe	Ni	Al	Si	Ti	B	C
Nominal	18.5	24.1	18.5	24.1	7.4	3.7	1.9	1.0	0.8
Measured DS	18.5±0.2	24.2±0.2	18.5±0.2	23.9±0.2	7.5±0.1	3.8±0.1	1.9±0.1	1.0±0.1	0.7±0.1
Measured CC	18.6±0.3	24.0±0.2	18.6±0.2	24.0±0.2	7.4±0.1	3.8±0.1	1.9±0.1	1.0±0.1	0.7±0.1

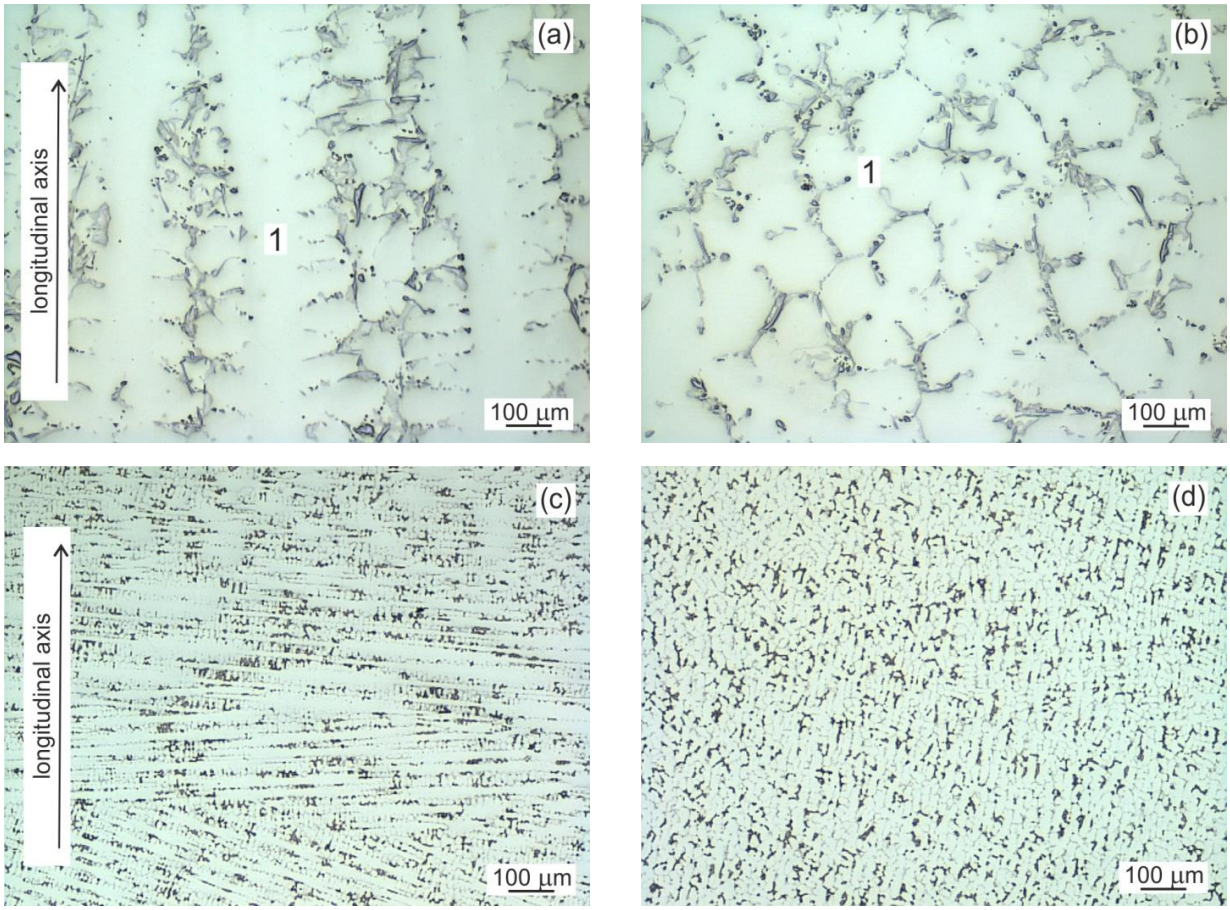

Figure 1 The typical microstructure of the DS and CC samples (LM): **(a)** Longitudinal section, DS; **(b)** Transversal sections, DS; **(c)** Longitudinal section, CC; **(d)** Central part of the transversal section, CC

Figure 1 shows the typical microstructure of DS and CC samples. The microstructure of both samples consists of dendrites (85 vol%) and interdendritic region (15 vol%). The columnar dendrites (1) in the DS sample grow in a direction parallel to the longitudinal axis of the DS ingot (**Figure 1(a)**). The average primary dendrite arm spacing (PDAS) and secondary dendrite arm spacing (SDAS) are measured to be (350 ± 8) µm and (90 ± 10) µm in the DS sample, respectively. The dendrites (1) show the typical fourfold crystal symmetry on the transversal section of the DS sample confirming that FCC(A1) is the primary solidification phase (**Figure 1(b)**). The columnar dendrites in the CC sample are inclined at an angle ranging from 70 to 90 degrees to the longitudinal axis of the CC ingot (**Figure 1(c)**). The central part of the CC sample consists of equiaxed dendrites indicating columnar-to-equiaxed transition (CET) during solidification (**Figure 1(d)**). The average PDAS and SDAS are measured to be (30 ± 5) µm and (9 ± 2) µm in the CC sample. A finer dendritic structure of the CC sample indicates that the cooling rate is significantly higher during CC process compared to that applied for the DS one [4].

Figure 2 shows the typical XRD pattern and microstructure of the studied samples. The XRD confirms only the presence of three phases such as FCC(A1), BCC(A2) and BCC(B2) (**Figure 2(a)**). Besides the dendrites

(1), four different areas designated as 2 to 5 can be well identified in the interdendritic region (**Figure 2(b)**). **Table 2** summarises the measured chemical composition of the identified areas. Based on the XRD, EDS, and taking into account the results of TEM analyses reported recently by Lapin et al. [13] for as-cast $Al_{0.4}Co_{0.9}Cr_{1.2}Fe_{0.9}$ $Ni_{1.2}(Si, Ti, C, B)_{0.375}$ CCA, the microstructure of the DS and CC samples consist of 1 - FCC(A1), 2 - BCC(B2)/BCC(A2), 3 - Cr_2B, 4 - TiC, and 5 - eutectics FCC(A1)+$(Ni, Co, Fe)_{16}(Ti, Cr)_6(Si, Al)_7$.

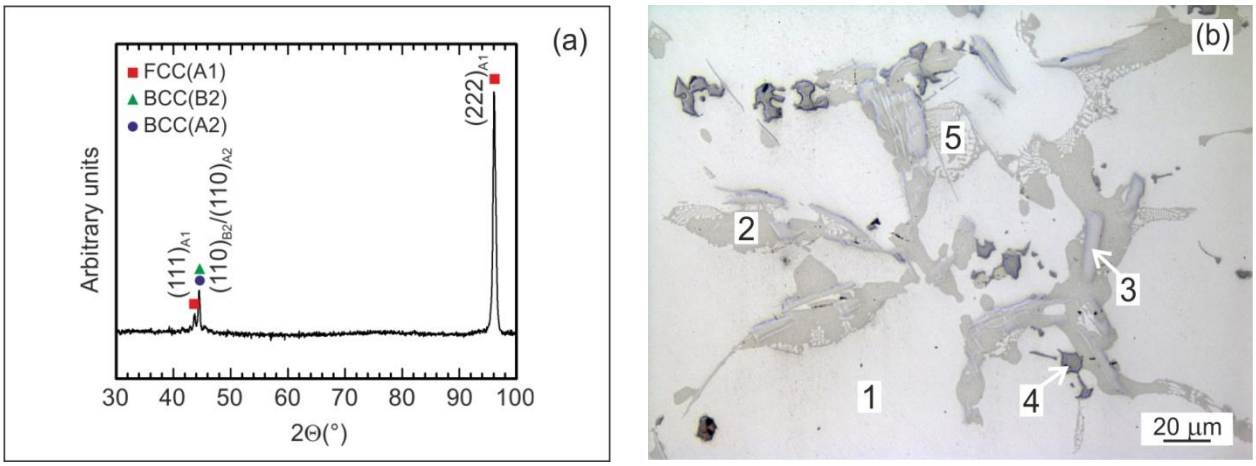

Figure 2 (a) The typical XRD pattern of the CC sample; **(b)** Coexisting phases in the DS sample: 1 - FCC(A1), 2 - BCC(B2)/BCC(A2), 3 - Cr_2B, 4 - TiC, 5 - eutectic FCC(A1)+$(Ni,Co,Fe)_{16}(Ti,Cr)_6(Si,Al)_7$

Table 2 Chemical composition of coexisting areas measured by EDS (at.%)

Area	Co	Cr	Fe	Ni	Al	Si	Ti	B	C
1	19.6±0.4	24.7±0.2	20.7±0.6	23.8±0.3	7.6±0.5	2.9±0.3	0.8±0.1	-	-
2	15.5±0.2	11.8±0.7	10.7±0.3	32.7±0.2	21.8±0.1	4.1±0.2	3.4±0.3	-	-
3	2.9±0.4	58.3±0.8	5.6±0.1	1.6±0.5	0.2±0.2	0.2±0.2	0.3±0.1	30.9±0.7	-
4	0.2±0.1	1.9±0.3	0.1±0.1	0.3±0.1	0,7±0.3	0,9±0.3	41.3±0.2	-	54.4±0.2
5	17.8±0.7	14.8±1.9	12.0±1.4	28.5±1.2	5.3±0.4	15.1±1.2	6.6±0.9	-	-

3.2 Microsegregation behaviour of alloying elements

The microsegregation behaviour of the alloying elements in the DS and CC samples can be described by the effective partition coefficient of the i-th element k_i defined as C_S^i/C_L^i, where C_S^i is the concentration of the i-th element in the solid and C_L^i is the concentration of the i-th element in the liquid. Since the multiphase interdendritic region of the DS and CC samples consists of coarse coexisting phases, the measurements of C_S^i and C_L^i were performed on the samples annealed at 1260 °C for 1 h, which were subsequently quenched into the water with a temperature of 20 °C (**Figure 3**). At the annealing temperature of 1260 °C, a full melting of the interdendritic phases is observed and the microstructure is significantly refined after the water quenching, as seen in **Figure 3(a)**. **Table 3** shows the positive segregation behaviour of Co and Fe into dendrites and the negative segregation behaviour of Al, Si, and Ti into interdendritic liquid. The alloying elements such as Cr and Ni show nearly equal partitioning between dendrites and interdendritic liquid for both DS and CC samples, as summarised in **Table 3**. The EDS line analysis for C and B across the interdendritic region marked by the yellow line in **Figure 3(b)** indicates their segregation to the interdendritic liquid during solidification, but the effective partition coefficients cannot be reliably calculated from these experimental measurements. It is worth noting that the effective partition coefficients measured for the DS and CC samples annealed at 1260 °C for 1 h are close to each other and vary only within standard deviations of the applied measurement method.

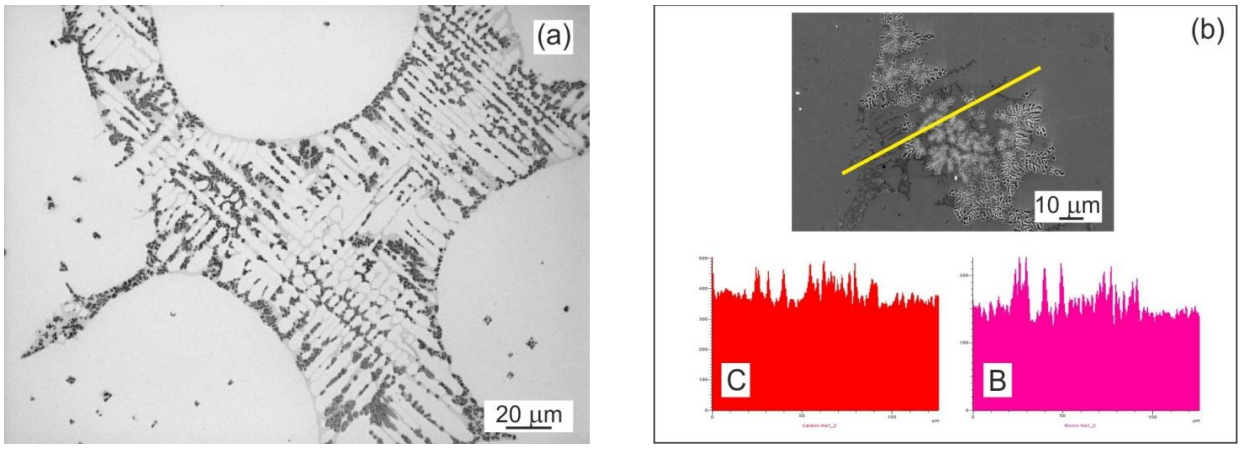

Figure 3 (a) The typical microstructure of the interdendritic region of the DS sample after annealing at 1260 °C followed by quenching; **(b)** Examples of EDS line analysis of C and B along the indicated yellow line

Table 3 The average chemical composition of dendrites C_S^i, the average chemical composition of the interdendritic region C_L^i, and effective partition coefficients k_i for the DS sample and CC sample

Element i	Co	Cr	Fe	Ni	Al	Si	Ti
DS sample							
C_S^i(at.%)	19.5±0.2	24.9±0.2	20.2±0.2	24.0±0.2	7.7±0.1	2.8±0.1	0.8±0.1
C_L^i(at.%)	17.6±0.2	24.7±0.2	15.5±0.2	24.9±0.2	8.2±0.1	5.4±0.1	3.7±0.1
k_i	1.11±0.02	1.01±0.01	1.30±0.02	0.96±0.02	0.94±0.01	0.51±0.01	0.23±0.01
CC sample							
C_S^i(at.%)	19.1±0.3	24.7±0.2	19.8±0.2	24.5±0.2	7.8±0.1	3.0±0.1	1.0±0.1
C_L^i(at.%)	17.2±0.2	24.8±0.2	15.3±0.3	24.6±0.2	8.1±0.1	5.8±0.1	4.3±0.1
k_i	1.12±0.02	1.00±0.01	1.29±0.02	0.99±0.02	0.96±0.01	0.52±0.01	0.23±0.01

4. CONCLUSION

The effect of two different solidification conditions on the microstructure formation and microsegregation behaviour of alloying elements in $Al_{0.4}CoCr_{1.3}FeNi_{1.3}(Si, Ti, C, B)_{0.4}$ complex concentrated alloy was studied. The microstructure of DS and CC samples consists of FCC(A1) dendrites and an interdendritic region composed of four areas with different chemical and phase compositions. A higher cooling rate during centrifugal casting leads to a much finer dendritic structure in the CC samples compared to that in the DS ones. The EDS line analysis and effective partition coefficients calculated from the measurements of the chemical composition of dendrites and interdendritic region in the DS and CC samples annealed at 1260 °C show preferential segregation of Al, Si, Ti, B and C to the interdendritic liquid during solidification at both studied solidification conditions.

ACKNOWLEDGEMENTS

This work was financially supported by Slovak Research and Development Agency under the contracts APVV-20-0505 and Slovak Grant Agency for Science under the contract VEGA 2/0018/22.

REFERENCES

[1] CANTOR, B., CHANG, I.T.H., KNIGHT, P., VINCENT, A.J.B.. Microstructural development in equiatomic multicomponent alloys. *Mater. Sci. Eng. A*. 2004, vol. 375-377, pp. 213-218. Available from: https://doi.org/10.1016/j.msea.2003.10.257.

[2] YEH, J.W., CHEN, S.K., LIN, S.J., GAN, J.Y., CHIN, T.S., SHUN, T.T., TSAU, C.H., CHANG, S.Y. Nanostructured high-entropy alloys with multiple principal elements: Novel alloy design concepts and outcomes. *Adv. Eng. Mater.* 2004, vol. 6, pp. 299-303. Available from: https://doi.org/10.1002/adem.200300567.

[3] GORSSE, S., MIRACLE, D.B., SENKOV, O.N. Mapping the world of complex concentrated alloys**.** *Acta Mater.* 2017, vol. 135, pp. 177-187. Available from: https://doi.org/10.1016/j.actamat.2017.06.027.

[4] STRYZHYBORODA, O., WITUSIEWICZ, V.T., GEIN, S., RÖHRENS, D., HECHT, U. Phase equilibria in the Al-Co-Cr-Fe-Ni high entropy alloy system: Thermodynamic description and experimental study. *Front. Mater.* 2020, vol. 7, pp. 1-13. Available from: https://doi.org/10.3389/fmats.2020.00270.

[5] RAO, J.C., DIAO, H.Y., OCELÍK, V., VAINCHTEIN, D., ZHANG, C., KUO, C., TANG, Z., GUO, W., POPLAWSKY, J.D., ZHOU, Y., LIAW, P.K., DE HOSSON, J.T.M. Secondary phases in Al_xCoCrFeNi high-entropy alloys: An in-situ TEM heating study and thermodynamic appraisal. *Acta Mater.* 2017, vol. 131, pp. 206-220. Available from: https://doi.org/10.1016/j.actamat.2017.03.066.

[6] YANG, T., XIA, S., LIU, S., WANG, C., LIU, S., ZHANG, Y., XUE, J., YAN, S., WANG, Y. Effects of Al addition on microstructure and mechanical properties of Al_xCoCrFeNi high-entropy alloy. *Mater. Sci. Eng. A.* 2015, vol. 648, pp. 15-22. Available from: https://doi.org/10.1016/j.msea.2015.09.034.

[7] KARLSSON, D., MARSHAL, A., JOHANSSON, F., SCHUISKY, M., SAHLBERG, M., SCHNEIDER, J.M., JANSSON, U. Elemental segregation in an AlCoCrFeNi high-entropy alloy - A comparison between selective laser melting and induction melting. *J. Alloys Compd.* 2019, vol. 784, pp. 195-203. Available from: https://doi.org/10.1016/j.jallcom.2018.12.267.

[8] MANZONI, A., DAOUD, H., VOLKL, R., GLATZEL, U., WANDERKA, N. Phase separation in equiatomic AlCoCrFeNi high-entropy alloy. *Ultramicroscopy.* 2013, vol. 132, pp. 212-215. Available from: https://doi.org/10.1016/j.ultramic.2012.12.015.

[9] FERRARI, V., WOLF, W., ZEPON, G., COURY, F.G., KAUFMAN, M.J., BOLFARINI, C., KIMINAMI, C.S., BOTTA, W.J. Effect of boron addition on the solidification sequence and microstructure of AlCoCrFeNi alloys. *J. Alloys Compd.* 2019, vol. 775, pp. 1235-1243. Available from: https://doi.org/10.1016/j.jallcom.2018.10.268.

[10] ASABRE, A., KOSTKA, A., STRYZHYBORODA, O., PFETZING-MICKLICH, J., HECHT, U. Effect of Al, Ti and C additions on Widmanstätten microstructures and mechanical properties of cast $Al_{0.6}$CoCrFeNi compositionally complex alloys. *Mater. Des.* 2019, vol. 184, 108201. Available from: https://doi.org/10.1016/j.matdes.2019.108201.

[11] CHEN, D., HE, F., HAN, B., WU, Q., TONG, Y., ZHAO, Y., WANG, Z., WANG, J., KAI, J. Synergistic effect of Ti and Al on $L1_2$-phase design in CoCrFeNi-based high entropy alloys. *Intermetallics*. 2019, vol. 110, 106476. Available from: https://doi.org/10.1016/j.intermet.2019.106476.

[12] ZHU, J.M., FU, H.M., ZHANG, H.F., WANG, A.M., LI, H., HU, Z.Q. Synthesis and properties of multiprincipal component AlCoCrFeNiSi_x alloys. *Mater. Sci. Eng. A*. 2010, vol. 527, pp. 7210-7214. Available from: https://doi.org/10.1016/j.msea.2010.07.049.

[13] LAPIN, J., KLIMOVÁ, A., PELACHOVÁ, T., ŠTAMBORSKÁ, M., BAJANA, O. Synergistic effect of Ti, B, Si, and C on microstructure and mechanical properties of as-cast $Al_{0.4}Co_{0.9}Cr_{1.2}Fe_{0.9}Ni_{1.2}(Si, Ti, C, B)_{0.375}$ complex concentrated alloy. *J. Alloys Compd.* 2023, vol. 93, 168050. Available from: https://doi.org/10.1016/j.jallcom.2022.168050.

[14] CUI, H., WANG, H., WANG, J., FU, H. Microstructure and microsegregation in directionally solidified FeCoNiCrAl high entropy alloy. *Adv. Mater. Res.* 2011, vol. 189-193, pp. 3840-3843. Available from: https://doi.org/10.4028/www.scientific.net/AMR.189-193.3840.

[15] ZHANG, Y., MA, S.G., QIAO, J.W. Morphology transition from dendrites to equiaxed grains for AlCoCrFeNi high-entropy alloys by copper mold casting and Bridgman solidification. *Metall. Mater. Trans. A*. 2012, vol. 43, pp. 2625-2630. Available from: https://doi.org/10.1007/s11661-011-0981-8.

[16] LIU, G., LIU, L., LIU, X., WANG, Z., HAN, Z., ZHANG, G., KOSTKA, A. Microstructure and mechanical properties of $Al_{0.7}$CoCrFeNi high-entropy-alloy prepared by directional solidification. *Intermetallics*. 2018, vol 93, pp. 93-100. Available from: https://doi.org/10.1016/j.intermet.2017.11.019.

[17] MA, S.G., ZHANG, S.F., QIAO, J.W., WANG, Z.H., GAO, M.C., JIAO, Z.M., YANG, H.J., ZHANG, Y. Superior high tensile elongation of a single-crystal CoCrFeNi$Al_{0.3}$ high-entropy alloy by Bridgman solidification. *Intermetallics*. 2014, vol. 54, pp. 104-109. Available from: https://doi.org/10.1016/j.intermet.2014.05.018.